ACS OMEGA

Open Access

http://pubs.acs.org/journal/acsodf

Article

Binding of Stimuli-Responsive Ruthenium Aqua Complexes with 9-Ethylguanine

Atsuki Maeda, Jun-ya Tokumoto, Soichiro Kojima, Keiichi Fujimori, Takayo Moriuchi-Kawakami, and Masanari Hirahara*

Cite This: *ACS Omega* 2023, 8, 37391−37401

Read Online

ACCESS | Metrics & More | Article Recommendations | Supporting Information

ABSTRACT: Stimuli-responsive ruthenium complexes *proximal*- and *distal*-[Ru(C_{10}tpy)(C_{10}pyqu) OH_2]$^{2+}$ (*proximal*-**1** and *distal*-**1**; C_{10}tpy = 4′-decyloxy-2,2′:6′,2″-terpyridine and C_{10}pyqu = 2-[2′-(6′-decyloxy)-pyridyl]quinoline) were experimentally studied for adduct formation with a model DNA base. At 303 K, *proximal*-**1** exhibited 1:1 adduct formation with 9-ethylguanine (9-EtG) to yield *proximal*-[Ru(C_{10}tpy)(C_{10}pyqu)(9-EtG)]$^{2+}$ (*proximal*-**RuEtG**). Rotation of the guanine ligand on the ruthenium center was sterically hindered by the presence of an adjacent quinoline moiety at 303 K. Results from ^{1}H NMR measurements indicated that photoirradiation of a *proximal*-**RuEtG** solution caused photoisomerization to *distal*-**RuEtG**, whereas heating of *proximal*-**RuEtG** caused ligand substitution to *proximal*-**1**. The distal isomer of the aqua complex, *distal*-**1**, was observed to slowly revert to *proximal*-**1** at 303 K. In the presence of 9-EtG, *distal*-**1** underwent thermal back-isomerization to *proximal*-**1** and adduct formation to *distal*-**RuEtG**. Kinetic analysis of ^{1}H NMR measurements showed that adduct formation between *proximal*-**1** and 9-EtG was 8-fold faster than that between *distal*-**1** and 9-EtG. This difference may be attributed to intramolecular hydrogen bonding and steric repulsion between the aqua ligand and the pendant moiety of the bidentate ligand..

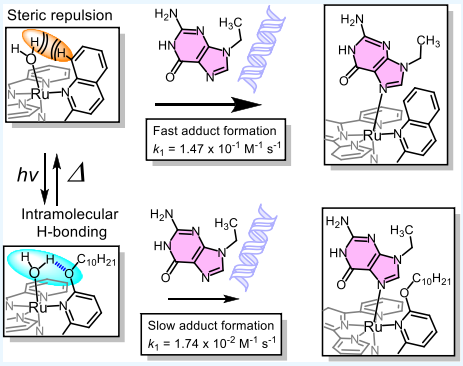

1. INTRODUCTION

Stimuli-responsive molecules have been studied extensively for their numerous potential applications, including a drug-delivery system,[1] catalysts,[2−4] molecular recognition,[5−7] and functional materials.[8−12] The key to stimulus responsiveness is molecular configurational changes (e.g., tautomerization and *cis*−*trans* isomerization). Among various external stimuli, light is a remote stimulus with high spatiotemporal controllability, making it applicable to bioactive systems.

Ruthenium complexes with polypyridyl ligands are promising candidates for the stimuli-responsive molecules.[13−16] These complexes absorb visible light because of the metal-to-ligand charge-transfer (MLCT) transition, followed by fast relaxation of singlet excited states to triplet MLCT (^{3}MLCT) states via a radiationless intersystem crossing.[17] The ^{3}MLCT excited states, which have submicrosecond lifetimes, have enabled applications in photoredox reactions,[18,19] artificial photosynthesis,[20−23] and electrochemiluminescence.[24] The ^{3}MLCT states show radiationless deactivation to ground states by thermal excitation to triplet metal-centered (^{3}MC) excited states and photodissociation of the ligand.[25,26] The five-coordinated intermediates allow substitution[26,27] or isomerization[14−16,28−31] reactions by coordinating other ligands. The photosubstitution reaction of the ruthenium complexes has been widely applied to light-activated metallodrugs[32−40] and photofunctional materials.[11,41]

We have studied photoresponsive ruthenium aqua complexes with tridentate and asymmetric bidentate ligands.[42−44] The introduction of a substituent near the metal center enhances the quantum yields of photoisomerization and allows thermal back isomerization from the distal to proximal isomer.[44] We have reported applications of these stimuli-responsive complexes to artificial photosynthesis,[45−47] stimulus-responsive giant vesicles,[48] host−guest systems.[13]

In this work, we focused on the ruthenium complex, *proximal*-[Ru(C_{10}tpy)(C_{10}pyqu) OH_2]$^{2+}$ (*proximal*-**1**), that responds to light and thermal stimuli (C_{10}tpy = 4′-decyloxy-2,2′:6′,2″-terpyridine and C_{10}pyqu = 2-[2′-(6′-decyloxy)-pyridyl]quinoline). The complex absorbed visible light and photoisomerized to *distal*-**1** (Scheme 1)[49] and thermal back-isomerized to *proximal*-**1**. The introduction of two long alkyl chains into both the tridentate and bidentate ligands can allow the immobilization of the molecule in lipid bilayers, which will have potential application to stimuli-responsive vesicles.[9,48] Furthermore, the introduction of long alkyl chains is expected

Received: July 24, 2023
Accepted: September 14, 2023
Published: September 26, 2023

Scheme 1. Photoisomerization and Thermal Back-Isomerization between *proximal*-1 and *distal*-1

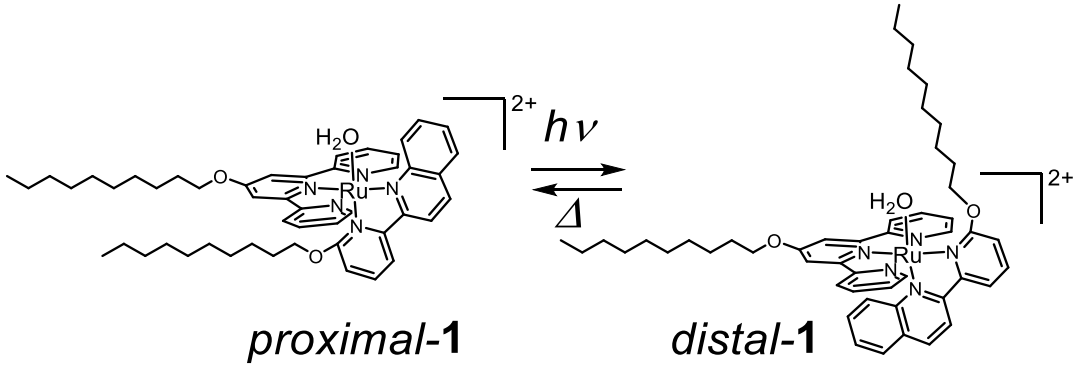

Scheme 2. Top: Synthetic Route (4 Steps) of C_{10}pyqu Starting from 2-Acetylpyridine[48,a]

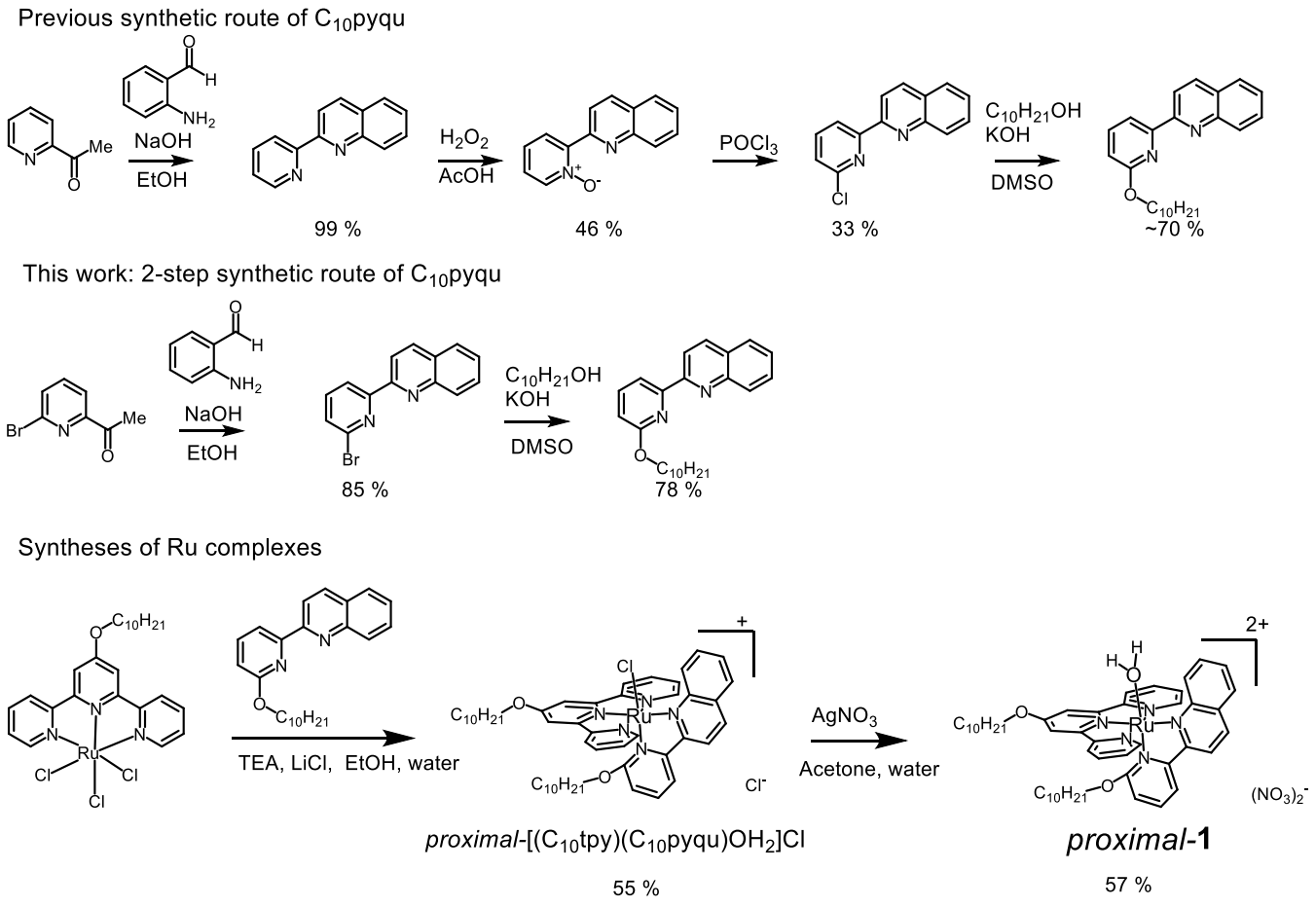

[a]Middle: 2-step syntheses of C_{10}pyqu in this work starting from 6-bromo-2-acetylpyridine. Bottom: synthetic route for Ru complexes. Adapted in part with permission from M. Hirahara (2016). Visible-light-induced morphological changes of giant vesicles by photoisomerization of a ruthenium aqua complex. *Chem. Eur. J.* **2016**, *22*, 2590−2594. Copyright 2016 Wiley-VCH GmbH.

to be developed as a metallodrug since lipophilicity of the complex correlates with cytotoxicity.[50,51] In this study, we report an external-stimuli-controlled ligand substitution reaction with a motif of a DNA structure. The binding studies of ruthenium complexes with simple model bases have attracted much attention because of their potential application in anticancer reagents.[52,53] Although photoresponsive ruthenium complexes for photoactivated chemotherapy have been reported by many groups,[32−40,54−60] photoresponsive-molecule-based ligand substitution reaction targeting DNA model bases has not been reported so far. Herein, we selected 9-ethylguanine and 9-methyladenine as base molecules, which have been reported to form a 1:1 or 1:2 adduct with ruthenium complexes.[52,61−63] Studies on NMR and UV−vis spectroscopy indicate that *proximal*-**1** exhibits ligand substitution with 9-ethylguanine in mixed aqueous solutions. The kinetic analysis revealed that the rate constant for the adduct formation in *proximal*-**1** is much faster than that in *distal*-**1** with 1 order of magnitude. Structural differences in the near reaction centers

https://doi.org/10.1021/acsomega.3c05343
ACS Omega 2023, 8, 37391−37401

of *proximal*- **1** and *distal*-**1** are presumed to be the cause of the difference in the rate constants.

2. EXPERIMENTAL SECTION

2.1. Materials. 4′-decyloxy-2,2′:6′,2″-terpyridine (C_{10}tpy),[48] [Ru(C_{10}tpy) Cl_3],[48] and *proximal*-[Ru(C_2tpy)-(C_2pyqu) OH_2]$(NO_3)_2$ (C_2tpy = 4′-ethoxy-2,2′:6′,2″-terpyridine; C_2pyqu = 2-(2′-(6′-ethoxy)-pyridyl) quinoline)[47] were prepared according to a reported procedure. 2-(2′-(6′-Decyloxy)-pyridyl) quinoline (C_{10}pyqu) was obtained from 2-(2′-(6′-bromo)-pyridyl) quinoline, which was obtained by a modified synthetic method from 2-aminobenzaldehyde and 2-acetyl-6-bromopyridine (Scheme 2). 9-Ethylguanine and 9-methyladenine were purchased from BLD Pharmatech Ltd. All other reagents were purchased and used without further purification. For binding studies with 9-EtG or 9-methyladenine, the nitrate salt of Ru complex, *proximal*-[Ru($C_n$tpy)-($C_n$pyqu) OH_2]$(NO_3)_2$ (n = 2, 10), was used.

2.2. Synthesis of Bidentate Ligands and Ruthenium Complexes. *2.2.1. 2-(2′-(6′-Bromo)-pyridyl) Quinoline.* 2-Aminobenzaldehyde (0.620 g, 5.1 mmol), 2-acetyl-6-bromopyridine (1.03 g, 5.2 mmol), and NaOH (0.629 g, 15.7 mmol) were added to a 200 mL round-bottom flask equipped with a stirring bar, and the reaction mixture was refluxed for 3 h. The reaction mixture was allowed to cool at room temperature, followed by adding 50 mL of water. The yellow precipitate was collected on a frit and washed with 20 mL of water. The yield was 0.896 g (61%). The filtrate was left at room temperature to give a second crop of the product (0.346 g, 24%). The precipitate was collected on a frit and dried under vacuum. The total yield was 1.242 g (85%). Both crops were spectroscopically identical. Anal. Calcd for 2-(2′-(6′-bromo)-pyridyl) quinoline, $C_{13}H_8BrN_3$: C, 54.57; H, 2.82; N, 14.69. Found: C, 54.41; H, 2.50; N, 14.50. ^{1}H NMR (400 MHz, $CDCl_3$): δ 8.64 (d, J = 7.7 Hz, 1H), 8.55 (d, J = 8.6 Hz, 1H), 8.28 (d, J = 8.6 Hz, 1H), 8.15 (d, J = 8.5 Hz, 1H), 7.86 (d, J = 8.4 Hz, 1H), 7.69−7.77 (m, 2H), 7.51−7.61 (m, 2H). ^{13}C NMR (101 MHz, $CDCl_3$): δ: 157.59, 154.58, 147.93, 141.64, 139.34, 137.05, 129.91, 129.83, 128.55, 128.44, 127.78, 127.19, 120.56, 119.14.

2.2.2. Modified Synthesis of 2-(2′-(6′-Decyloxy)-pyridyl) Quinoline (C_{10}pyqu). 2-(2′-(6′-Bromo)-pyridyl) quinoline (0.523 g, 1.85 mmol), 1-decanol (5.29 g, 33.4 mmol), KOH (3.06 g, 55.6 mmol), and DMSO (35 mL) were added to a 200 mL round-bottom flask with a stirring bar. The reaction mixture was heated to 80 °C for 20 h and then cooled to room temperature. Half of the yellow solution was transferred to a 500 mL separate funnel with deionized water (100 mL). The organic layer was thoroughly extracted with hexane (50 mL × 5). The other half of the sample was also extracted with hexane (50 mL × 5). The combined organic layers (ca. 500 mL) were evaporated to give a yellow oil with a yield of 5.26 g. The oil contained significant amounts of 1-decanol (C_{10}pyqu/1-decanol = 1:21) according to the peak integrals in the ^{1}H NMR spectrum. The mixture was used in the next reaction without removing excess 1-decanol. The product yield was estimated to be 78% from the apparent molecular weight of the product (app. MW = 3640 g/mol).[64] ^{1}H NMR (300 MHz, $CDCl_3$): δ 8.54 (d, J = 8.6 Hz, 1H), 8.21−8.29 (d, 2H), 8.16 (d, J = 8.3 Hz, 1H), 7.85 (dd, J = 8.0, 1.5 Hz, 1H), 7.67−7.79 (m, 2H), 7.49−7.58 (m, 1H), 6.81 (dd, J = 8.2, 0.8 Hz, 1H), 4.47 (t, J = 6.7 Hz, 2H), 1.84 (2H, overlapping with 1-decanol), 0.61−1.71 (m, overlapping with 1-decanol).

2.2.3. Modified Synthesis of proximal-[Ru(C_{10}tpy)-(C_{10}pyqu) Cl]Cl. [Ru(C_{10}tpy) Cl_3] (851 mg, 1.45 mmol), LiCl (645 mg), triethylamine (0.635 g), EtOH (109 mL), and water (36 mL) were added to a 200 mL round-bottom flask with a mixture of C_{10}pyqu and 1-decanol (5.26 g, C_{10}pyqu/1-decanol = 1:21). The mixture was refluxed for 2 days, and the progress of the reaction was monitored by thin-layered chromatography (eluent/methanol and ethyl acetate, 1:8, v/v). The purple spot representing the product appeared at R_f = 0.2, whereas a red spot representing the byproduct [Ru-(C_{10}tpy)$_2$]$^{2+}$ appeared at R_f = 0.05. After the reaction, the mixture was evaporated to give a purple oil, and ether was added until a purple precipitate formed. The suspension was collected on a glass frit and dried under vacuum. The crude product (1.4 g) was transferred to a 200 mL Erlenmeyer flask, and acetone (50 mL) was added. The suspension was sonicated for 1 min and left for 5 min. After decantation, the purple supernatant was transferred to a beaker. Additional acetone (50 mL) was added to the remaining solid and sonicated. The same decantation process was repeated three times. The combined acetone extracts were evaporated to dryness. The yield was 0.711 g (55.3%). ^{1}H NMR of the product contained small amounts of impurities that may have been derived from *distal*-[Ru(C_{10}tpy)(C_{10}pyqu) Cl]Cl, but it was used in the next reaction without further purification.

*2.2.4. proximal-[Ru(C_{10}tpy)(C_{10}pyqu) OH_2]$(NO_3)_2$ (proximal-[**1**]$(NO_3)_2$).* *proximal*-[Ru(C_{10}tpy)(C_{10}pyqu) Cl]Cl (679 mg, 0.735 mmol), 0.1 M $AgNO_3$ (32 mL, 3.2 mmol), acetone (65 mL), and water (21 mL) were added to a 200 mL flask. The mixture was refluxed overnight and filtered through Celite. Saturated aqueous solution of $NaNO_3$ (0.2 mL) was added to the filtrate, and the solution was evaporated until a purple solid was precipitated. The solid was collected on a frit and washed with deionized water. Yield 451 mg (56.7%). ^{1}H NMR and ESI MS spectra of the product showed good agreement with that reported previously.[48]

*2.2.5. Isolation of proximal-[Ru(C_{10}tpy)(C_{10}pyqu)(9-ethylguanine)]$(PF_6)_2$ (proximal-[**RuEtG**]$(PF_6)_2$).* 9-Ethylguanine (10.8 mg, 0.060 mmol) and *proximal*-[**1**]$(NO_3)_2$ (10.0 mg, 0.010 mmol), TFE (0.016 mL), methanol (1.3 mL), and water (0.60 mL) were added in a 20 mL glass vial. The mixture was stirred for 2 days at room temperature. A saturated aqueous solution of NH_4PF_6 (∼0.1 mL) was added to the solution, and the solution was stirred for 1 h. The solid was collected on a glass frit and washed with minimum amount of water. The yield was 8.9 mg (64%). ^{1}H NMR (400 MHz, acetone-d_6): δ 8.97−8.78 (m, 3H), 8.67 (s, 1H), 8.49 (d, J = 8.1 Hz, 1H), 8.43 (d, J = 5.5 Hz, 1H), 8.29 (d, J = 8.1 Hz, 1H), 8.26 (s, 1H), 8.22−8.15 (m, 2H), 8.04 (d, J = 6.3 Hz, 1H), 7.93 (t, J = 8.2 Hz, 1H), 7.82 (t, J = 8.2 Hz, 1H), 7.76 (d, J = 8.9 Hz, 1H), 7.62 (t, J = 7.6 Hz, 1H), 7.49 (t, J = 6.5 Hz, 1H), 7.34−7.25 (m, 2H), 7.21 (t, J = 6.5 Hz, 1H), 6.85 (d, J = 8.4 Hz, 1H), 6.09 (s broad, 1H). ESI MS of *proximal*-[**RuEtG**]$(PF_6)_2$ (solvent: H_2O/methanol/TFE = 70/50/2, v/v/v) m/z (calcd): 516.31 (516.22, [M − 2(PF_6)]$^{2+}$). Elemental analysis was not measured since the product contains ∼10% of *proximal*-**1** according to the integration of peaks in the ^{1}H NMR spectrum.

2.3. Measurements. ^{1}H NMR spectra were recorded on a JEOL 400 or Varian 270 MHz spectrometer. ^{1}H NMR spectra were referenced by using the residual proton signal of CD_3OD as an internal standard. The residual HDO peak was presaturated to improve the S/N ratio. Visible-light irradiation

https://doi.org/10.1021/acsomega.3c05343
ACS Omega 2023, 8, 37391−37401

of NMR samples for at least 90 min was performed using a halogen lamp (MegalLight 100 V, >390 nm, 19 mW cm^{-2}). All NMR data were analyzed using MestReNova, and kinetic traces were fitted using Copasi software.

Absorption spectra were recorded with a Hitachi U2910 spectrophotometer equipped with a temperature controller. The sample solution in the cuvette was irradiated with collimated light (F220SMA-A, Thorlab, ϕ = ~5 mm) from the top of the solution. The collimator was connected to a blue LED (M470F3, Thorlab, 14 mW cm^{-2}) and an LED controller (DC2200, Thorlab) through optical fibers (ϕ = 400 μm, SMA−SMA fiber, Thorlab). For time-course experiments, initiation of the measurement and LED-light irradiation were triggered by Microsoft power automate. Absorption spectra were analyzed with Spectragryph software[65] and plotted with Origin 2020b (OriginLab Corp., Northampton, MA, USA). Electrospray ionization time-of-flight mass spectra were obtained for a mixed aqueous solution of the complexes using a JEOL JMS-T100CS.

3. RESULTS AND DISCUSSION

3.1. Absorption Spectral Changes of *proximal*-1 in the Presence of 9-Ethylguanine. The adduct formation reaction was studied by mixing an aqueous solution of the ruthenium aqua complex (*proximal*-**1**, 29 μM) and 570 μM 9-ethylguanine (9-EtG) at 303 K in the dark. The substitution reactions of *proximal*-**1** with the base molecule can be expressed by eq 1

$$\underset{\text{proximal-1}}{\text{proximal}-[(C_{10}\text{tpy})(C_{10}\text{pq})OH_2]^{2+}} + \underset{\text{9-EtG}}{9-\text{ethylguanine}} \rightleftharpoons \underset{\text{proximal-RuEtG}}{\text{proximal} - [(C_{10}\text{tpy})(C_{10}\text{pq})(9-\text{EtG})]^{2+}} + H_2O \quad (1)$$

Absorption spectra and kinetic traces at 550 nm during the reaction are depicted in Figure 1. The MLCT band at 521 nm decreased, while a new absorption band appeared at 512 nm with an isosbestic point at 516 nm, and the kinetic traces were fitted with a single exponential curve (Figure 1B). In the presence of 570 μM of 9-EtG, the pseudo-first-order rate constant8 k_{obs} was determined to be 1.91 ± 0.06 × 10^{-4} s^{-1}. As the concentration of 9-EtG increased, k_{obs} increased linearly (Figure 1D). In the presence of excess 9-EtG, second-order rate constants k_1 (for the adduct formation) and k_{-1} (for the reverse aquation reaction) were derived from the plot of k_{obs} vs [9-EtG] as expressed by eq 2

$$k_{obs} = k_1[9 - \text{EtG}] + k_{-1} \quad (2)$$

The second-order rate constant (k_1) for the adduct formation and a rate constant for backward reaction (k_{-1}) were estimated to be 1.7 ± 0.2 × 10^{-1} M^{-1} s^{-1} and 8 ± 3 × 10^{-5} s^{-1} at 303 K from the slope of the plot (Figure 1D), respectively. The same reaction was examined by adding 9-methyladenine; however, no spectral changes in UV−vis spectra were observed after 24 h (Figure S1). ESI-MS spectra after the adduct formation with 9-EtG showed a peak at 516.3 m/z (Figure 2) derived from the dicationic ruthenium complex, which is in good agreement with the isotope pattern of $[Ru(C_{10}tpy)(C_{10}pyqu)(9\text{-EtG})]^{2+}$. A dicationic peak corresponding to $[Ru(C_{10}tpy)(C_{10}pq)]^{2+}$ (m/z = 426.7) was observed as a minor peak, indicating that the adduct with 9-EtG is the major species formed in the reaction (Figure 2).

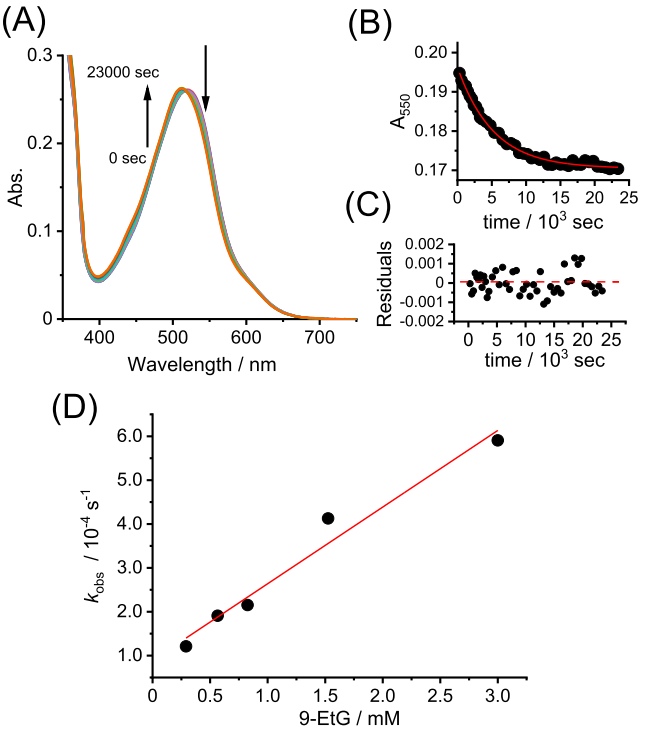

Figure 1. (A) Absorption spectral changes of *proximal*-**1** (29 μM) in the presence of 9-EtG (570 μM, 20 equiv) at 303 K. Solvent: H_2O/CH_3OH/2,2,2-trifluoroethanol (TFE) = 70:50:2, v/v/v. (B) Absorbance changes at 550 nm (black dot) during the reaction and fitting curve (solid line) based on the pseudo-first-order reaction model. (C) Residual plots for the fitting curve. (D) Concentration dependency of the observed rate constants (k_{obs}) for the ligand substitution reaction of *proximal*-**1** with 9-EtG at 303 K.

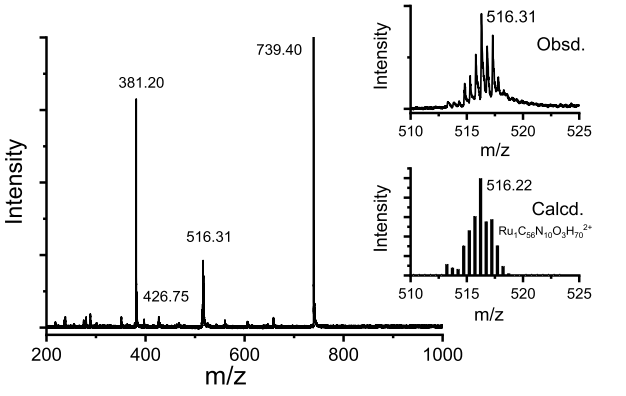

Figure 2. ESI-MS spectra of $[Ru(C_{10}tpy)(C_{10}pq)(9\text{-EtG})]^{2+}$. Conditions: *proximal*-**1** (0.1 mM) and 9-ethylguanine (2 mM) in mixed solvents (H_2O/methanol/TFE = 70/50/2, v/v/v). The sample solution was left at room temperature in the dark for 24 h to complete the ligand substitution reaction. Peaks at 381.20 and 739.40 m/z correspond to the ionized species of $[(9\text{-EtG})_2 + Na]^+$ and $[(9\text{-EtG})_4 + Na]^+$, respectively. Inset: observed spectra at 516 m/z and calculated isotope pattern of $[Ru(C_{10}tpy)(C_{10}pq)(9\text{-EtG})]^{2+}$.

Similar kinetic measurements were performed using *proximal*-$[Ru(C_2tpy)(C_2pyqu)(OH_2)]^{2+}$ and 570 μM 9-EtG (Figure S2). The observed rate constant for adduct formation was estimated to be 1.78 ± 0.03 × 10^{-4} s^{-1}, indicating that the length of the alkyl chains does not affect adduct formation.

3.2. ^{1}H NMR Studies of the Adduct Formation between *proximal*-1 and 9-EtG. ^{1}H NMR spectra of a

https://doi.org/10.1021/acsomega.3c05343
ACS Omega 2023, 8, 37391−37401

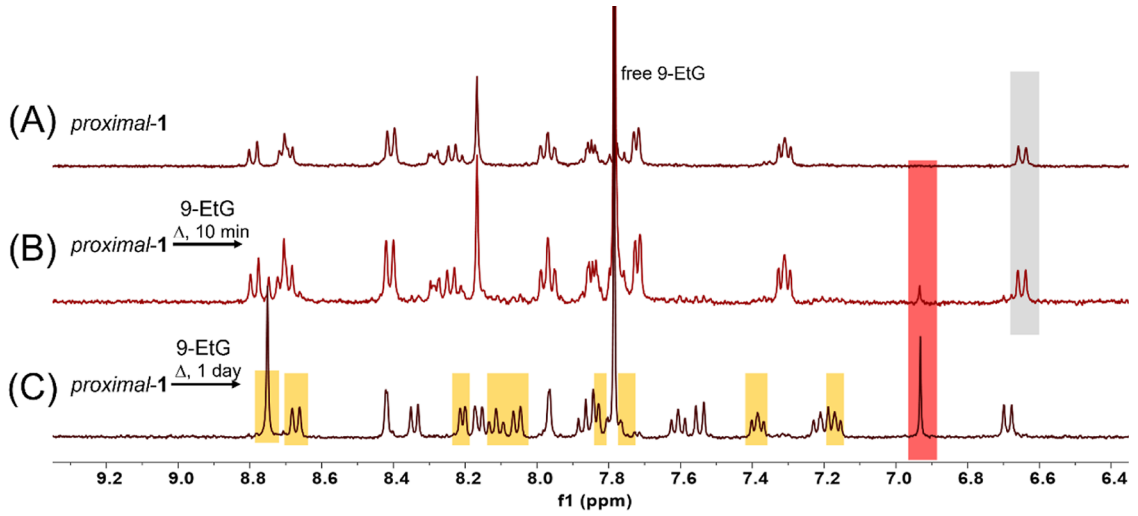

Figure 3. ^{1}H NMR spectra of (A) *proximal*-**1** (B) 10 min after mixing *proximal*-**1** (1 mM) with 9-EtG (5 mM) and (C) *proximal*-**1** and 9-EtG after incubation for 1 day. Peaks associated with *proximal*-**1** at 6.64 ppm and *proximal*-**RuEtG** at 6.93 ppm are colored gray and red, respectively. In (C), peaks corresponding to aromatic protons of C_{10}tpy of *proximal*-**RuEtG** are highlighted with yellow. Solvent: D_2O/CD_3OD/2,2,2-trifluoroethanol (TFE) = 70:50:2, v/v/v. The singlet at 7.8 ppm corresponds to the C−H proton of the free 9-EtG.

mixed aqueous solution of *proximal*-**1** (1 mM) and 9-EtG (5 mM) are shown in Figure 3. 10 min after mixing the two reagents, a singlet peak at 6.93 ppm appeared, and the peak intensity increased during the reaction (Figure 3B,C). After incubation at 303 K for 1 day, the peak corresponding to *proximal*-**1** became very weak, and new peaks were observed, including a singlet peak for one proton at 6.93 ppm. According to ^{1}H−^{1}H COSY measurements (Figure S3), this singlet peak was identified as the aromatic C−H proton of 9-EtG. The ^{1}H NMR spectrum of *proximal*-**1** and 9-EtG after 1 day of incubation yielded peaks of the product, a singlet peak from unreacted 9-EtG (Figure 3C), and *proximal*-**1** as a minor component, which is consistent with the ESI-MS spectral results (Figure 2). The above results support the formation of the adduct from *proximal*-**1** to *proximal*-[Ru(C_{10}tpy)(C_{10}pq)-(9-EtG)]$^{2+}$ (*proximal*-**RuEtG**). Chemical shifts of protons at position 8 in free 9-EtG (7.78 ppm) shifted by 0.86 ppm after the adduct formation. This large shift may indicate the coordination with N7 nitrogen to the Ru center. NOESY and ROESY spectra were taken to observe the correlation with the C−H proton o-f 9-EtG with the bidentate ligand. However, no correlation was observed due to the limitations of solubility of the complex. Fitting the kinetic traces in Figure 4 based on reaction eq 2 gave rate constants of k_1 (1.56 ± 0.03 × 10^{-1} M^{-1} s^{-1}) and k_{-1} (1.7 ± 0.1 × 10^{-4} s^{-1}), respectively. These kinetic constants have good agreement with the values obtained from UV−vis absorption spectra measurements (k_1 = 1.7 ± 0.2 × 10^{-1} M^{-1} s^{-1} and k_1 = 8 ± 3 × 10^{-5} s^{-1}). The ratio of *proximal*-**1** and *proximal*-**RuEtG** was 82:18 according to the integration of peaks at 6.93 (*proximal*-**RuEtG**) and 6.63−6.72 (*proximal*-**1** and *proximal*-**RuEtG**) ppm. The equilibrium constant (K = [*proximal*-**RuEtG**]/([*proximal*-**1**][9-EtG])) was estimated to be 1.24 ± 0.18 × 10^{3} M^{-1} based on the integration of the peak at four concentrations of 9-EtG (1.4, 2.7, 3.8, and 5.0 mM).

In the ^{1}H NMR spectrum of the product, *proximal*-**RuEtG**, protons of C_{10}tpy were characterized by ^{1}H−^{1}H COSY spectra (Figure S3) in the presence of 5 mM of 9-EtG. Peaks of aromatic C−H proton of C_{10}tpy appeared asymmetrically (Figure 3C), which is contrastive to C_{2v} symmetric aromatic

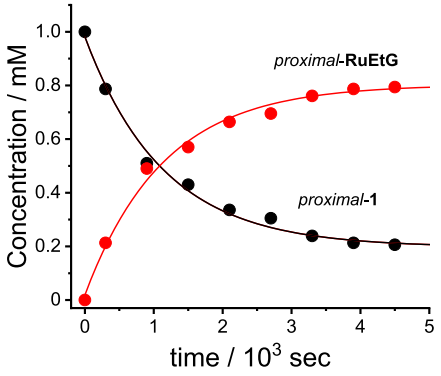

Figure 4. Kinetic traces of *proximal*-**1** (1 mM) during the substitution reaction with 5 mM 9-EtG at 303 K. Red: *proximal*-**RuEtG**; black: *proximal*-**1**. The concentrations of the complexes were calculated by integrating peaks at 6.92 ppm (*proximal*-**RuEtG**) and 6.63−6.70 ppm (*proximal*-**1** and *proximal*-**RuEtG**).

protons of C_{10}tpy in *proximal*-**1**. The isolated salt of *proximal*-**RuEtG** also showed asymmetric terpyridine peaks in d-acetone (Figure S4). The multiplicity of the peak arises from the two side pyridine rings of C_{10}tpy being inequivalent to each other. The asymmetry of the tridentate ligand indicates that rotation of 9-EtG along the axial axis is prevented at this temperature, which contrasts with the reported free rotation of 9-EtG in a ruthenium complex with tridentate and bidentate ligands.[52] VT-NMR spectra (303−333 K) showed no spectral change with respect to the symmetry of the C_{10}tpy ligand. Instead, the peaks corresponding to *proximal*-**1** increased in intensity, indicating a thermal reverse substitution reaction from *proximal*-**RuEtG** to *proximal*-**1** (Figure S5).

3.3. Adduct Formation between *distal*-1 and 9-EtG.

The ligand substitution reactions were investigated after light irradiation of mixed aqueous solutions of the ruthenium aqua complexes. As reported previously, *proximal*-**1** photoisomerizes to *distal*-**1** to yield a mixture of the two isomers in the photostationary state. Furthermore, ^{1}H NMR measurements have shown that *distal*-**1** undergoes thermal back-isomerization to *proximal*-**1** at ambient temperature.[13,48] Absorption spectra

https://doi.org/10.1021/acsomega.3c05343
ACS Omega 2023, 8, 37391−37401

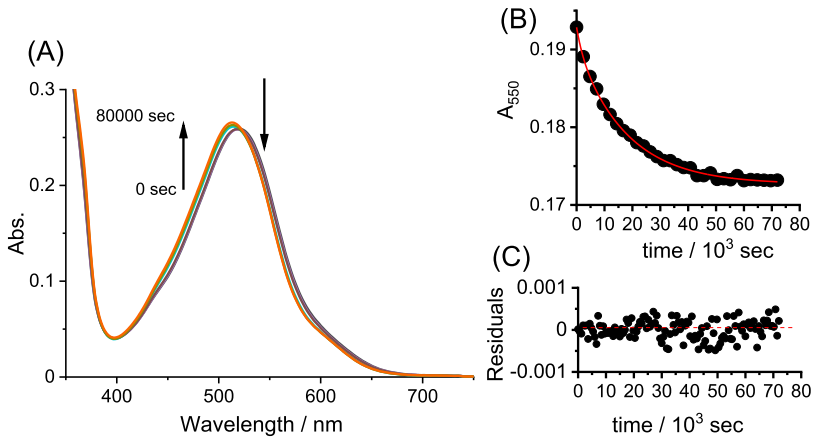

Figure 5. (A) Absorption spectral changes of *proximal*- and *distal*-**1** (28.3 μM) in the presence of 9-EtG (566 μM, 20 equiv) at 303 K. (B) Kinetic profile (black dot) during the reaction and fitting curve (red line) based on the double exponential curve. (C) Residual plots for the fitting curve. Solvent: $D_2O/CD_3OD/TFE$ = 70:50:2, v/v/v.

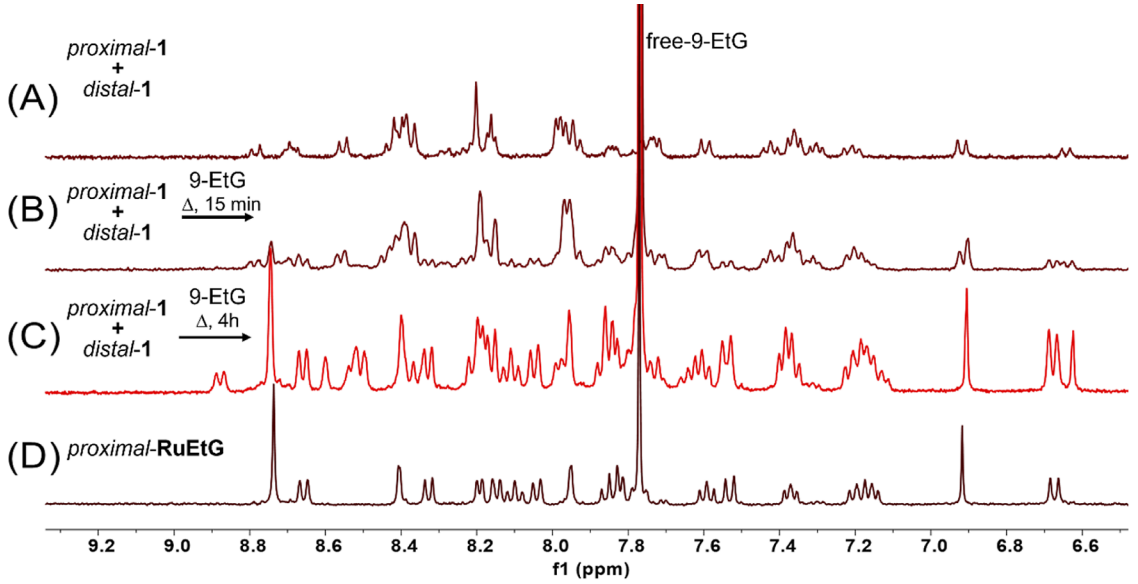

Figure 6. ^{1}H NMR spectral changes during the substitution reaction of *proximal*-**1** and *distal*-**1** with 9-EtG in the dark at 303 K. (A) *Proximal*-**1** and *distal*-**1** in the photostationary state. (B) *Proximal*-**1** and *distal*-**1** (1 mM) after 15 min of mixing with 9-EtG (5 mM). (C) *Proximal*-**1** and *distal*-**1** after 4 h of mixing with 9-EtG. (D) *Proximal*-**RuEtG**. Solvent: $D_2O/CD_3OD/TFE$ = 70:50:2, v/v/v.

during the thermal back-reaction using an aqueous solution of *proximal*-**1** and *distal*-**1** in the photostationary state are shown in Figure S6. The observed rate constant for spectral changes is $3.96 \pm 0.03\times 10^{-5}$ s^{-1}, which is near-identical to the value obtained from ^{1}H NMR spectroscopy[13] (4.0×10^{-5} s^{-1}) at the same temperature (303 K).

We then reacted the mixture of *proximal*-**1** and *distal*-**1** with 9-EtG, and the progress of the reaction was monitored by UV−vis spectroscopy (Figure 5). Kinetic traces, Figure 5B, were well-fitted with double exponential curves, with rate constants determined as $4.6 \pm 1.1 \times 10^{-4}$ and $5.6 \pm 0.1 \times 10^{-5}$ s^{-1}. Detailed kinetics were not distinguishable because this reaction system contained two ligand substitution reactions and a thermal back-isomerization reaction, with each complex yielding a similar absorption profile.

^{1}H NMR spectra were recorded for the reaction of *proximal*- and *distal*-**1** with 9-EtG, as depicted in Figure 6. The mixture of the isomers was prepared in situ by light irradiation to *proximal*-**1** prior to measurement. At 15 min after mixing, the doublet peak of *distal*-**1** at 6.92 ppm and the singlet peak of *proximal*-**RuEtG** are observed to be in partial overlap (Figure 6B). This *distal*-**1**-derived peak was essentially absent after 4 h. In the ^{1}H NMR spectrum after 4 h of mixing with 9-EtG, a doublet peak at 8.90 ppm and a singlet peak at 6.60 ppm were observed as a minor component, and these peaks were also observed after light irradiation of a *proximal*-**RuEtG** solution. These results indicate that the newly appearing peaks arise from *distal*-**RuEtG**. The singlet at 6.6 ppm after 4 h of mixing with 9-EtG (Figure 6C) was characterized as the C−H proton on the coordinated 9-EtG of *distal*-**RuEtG**. The thermal isomerization reaction between 9-EtG adducts (*proximal*-**RuEtG** and *distal*-**RuEtG**) can be considered negligible since no *distal*-**RuEtG**-derived peaks appeared after incubation of the solution of *proximal*-**RuEtG** (Figure S5).

The concentrations of the four complexes were calculated by integrating peaks at 8.90, 8.80, 6.92, and 6.70 ppm in Figure 6. In each measurement, the total concentration of the complexes was approximately constant. Integrating peaks at 6.62 and 6.92

https://doi.org/10.1021/acsomega.3c05343
ACS Omega 2023, 8, 37391−37401

ppm gave a *proximal*-**1**/*distal*-**1** ratio of 45:55 before mixing with 9-EtG. After 4 h of mixing with 9-EtG, the *proximal*-**RuEtG**/*distal*-**RuEtG** ratio was 78:22 (Figure 7), indicating

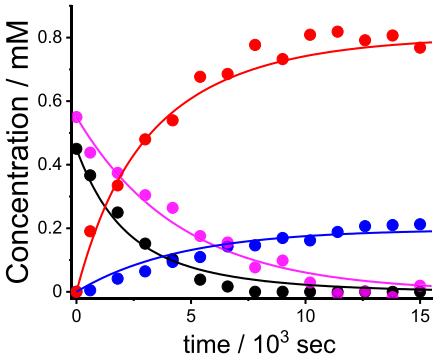

Figure 7. Kinetic traces of *proximal*-**1** and *distal*-**1** (total concentration: 1 mM) during the substitution reaction with 9-EtG (5 mM) at 303 K. Red: *proximal*-**RuEtG**; blue: *distal*-**RuEtG**; magenta: *distal*-**1**; black: *proximal*-**1**. The concentration of each complex was calculated based on the integration of peaks at 8.90 ppm (*distal*-**RuEtG**), 8.80 ppm (*proximal*-**1**), 6.92 ppm (*distal*-**1** and *proximal*-**RuEtG**), and 6.63−6.70 ppm (*proximal*-**1**, *proximal*-**RuEtG** and *distal*-**RuEtG**). The solid lines are simulated curves according to first-order kinetics based on ligand substitution (*proximal*-**1** to *proximal*-**RuEtG**, *distal*-**1** to *distal*-**RuEtG**) and thermal isomerization (*distal*-**1** to *proximal*-**1**) reactions.

that thermal back-isomerization from *distal*-**1** to *proximal*-**1** was occurring in the reaction. The kinetic traces in Figure 7 were analyzed based on the reaction model shown in Scheme 3; formation of the two guanine adducts (*proximal*-**1** to *proximal*-**RuEtG** and *distal*-**1** to *distal*-**RuEtG**) and thermal back-isomerization (*distal*-**1** to *proximal*-**1**). Fitting the kinetic traces (solid lines in Figure 7) based on the model in Scheme 3 showed good agreement with experimental data (dotted plots in Figure 7). The second-order rate constants of the adduct formation were estimated to be $1.47 \pm 0.07 \times 10^{-1}$ and $1.74 \pm 0.07 \times 10^{-2}$ M^{-1} s^{-1} for *proximal*-**1** to *proximal*-**RuEtG** and *distal*-**1** to *distal*-**RuEtG**, respectively. The rate constant for thermal back-isomerization was estimated to be $1.46 \pm 0.06 \times 10^{-4}$ s^{-1}. The traces were also examined to fit with the reversible adduct formation model in a similar manner to the kinetic analysis for adduct formation between *proximal*-**1** and 9-EtG. However, the kinetic constants for the reverse reaction were not obtained. This may be due to the difficulty of the lower concentrations of free ruthenium aqua complexes whose concentrations are less than 0.05 mM under the conditions employed. The adduct formation reaction was examined *proximal*-/and *distal*-**1** with 9-methyladenine, but only thermal back-isomerization of the aqua complex was observed (Figure S7).

3.3.1. Difference in Reactivity between Isomers in Adduct Formation. The observed rate constants for the two adduct formation reactions with 9-EtG differed by an order of magnitude between the isomers. This major difference between the two isomers may be attributed to the steric hindrance and intramolecular hydrogen bonding between the aqua ligand and the bidentate ligand, as shown in the model in Scheme 3. We have reported previously the crystal structures of similar complexes, *proximal*-$[Ru(C_2tpy)(C_2pyqu)\ OH_2]^{2+}$ and *distal*-$[Ru(C_2tpy)(C_2pyqu)\ OH_2]^{2+}$, with shorter alkyl

Scheme 3. Binding Reactions with 9-EtG for the Stimuli-Responsive Ruthenium Complexes *proximal*-1 and *distal*-1[a]

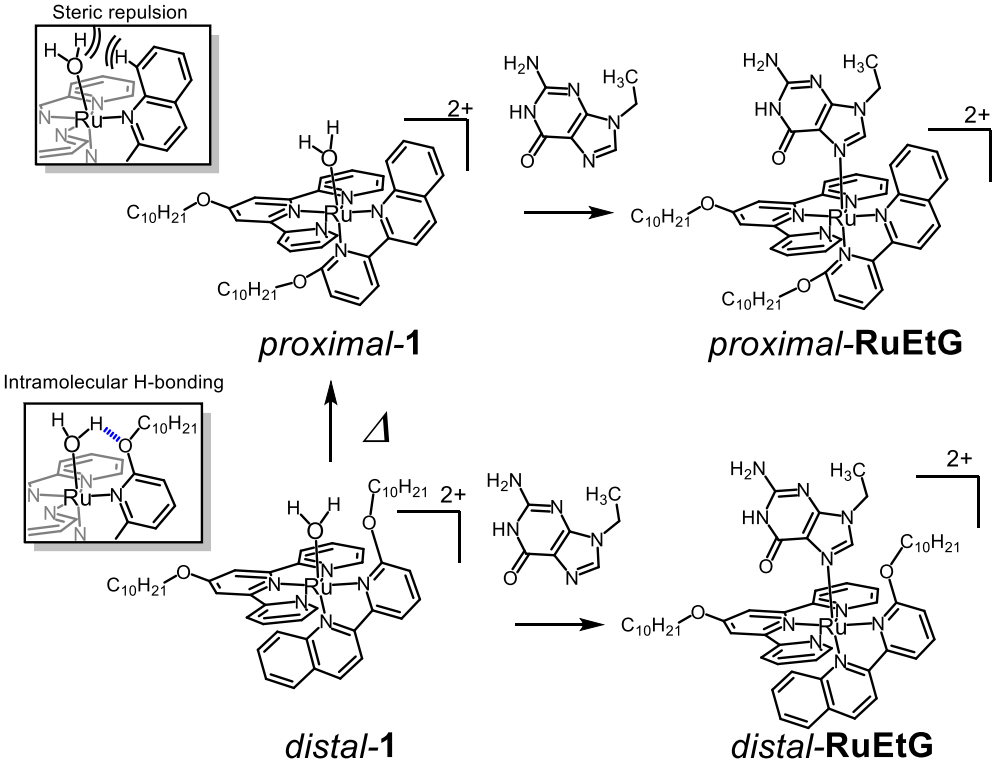

[a]The insets show steric repulsion between the aqua ligand and quinoline moiety in *proximal*-**1** and intramolecular hydrogen bonding between the aqua ligand and alkoxy unit in *distal*-**1**.

https://doi.org/10.1021/acsomega.3c05343
ACS Omega 2023, 8, 37391−37401

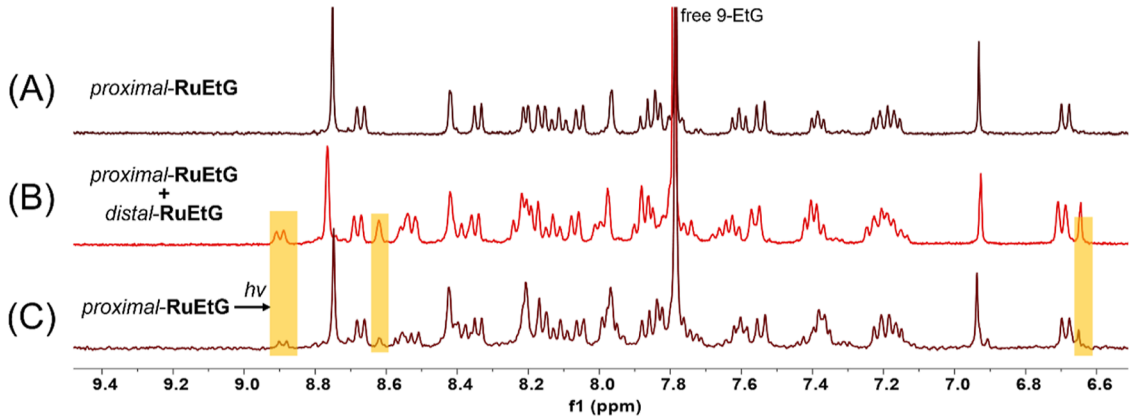

Figure 8. ^{1}H NMR spectra of (A) *proximal*-**RuEtG**, (B) *proximal*- and *distal*-**RuEtG**, and (C) *proximal*-**RuEtG** after visible light irradiation for 16 h. Representative peaks of *distal*-RuEtG are highlighted as yellow. Solvent: $D_2O/CD_3OD/TFE$ = 70:50:2, v/v/v.

chains than *proximal*-**1**.[47] The aqua ligand displayed steric repulsion between the aqua ligand quinoline moiety in *proximal*-$[Ru(C_2tpy)(C_2pyqu)\ OH_2]^{2+}$ where the dihedral angle of the O−Ru−N−C is 24.6(2)° and the distance between the aqua ligand and C8 quinoline carbon is 3.114(7) Å. In contrast, *distal*-$[Ru(C_2tpy)(C_2pyqu)\ OH_2]^{2+}$ exhibited intramolecular hydrogen bonding with the oxygen atom of the ethoxy substituent, where the O1···O3 distance is 2.640(3) Å and the O3−N4−Ru1−O1 torsion angle is 14.91(12)°. Therefore, steric repulsion in *proximal*-**1** (Scheme 3) may have caused a faster ligand substitution reaction than that in *distal*-**1**. Increases in the reaction rate of ligand substitution reactions by steric hindrance between ligands have been reported previously in ruthenium complexes with bulky bidentate ligands.[66,67] Our previous studies have also shown that the presence of steric hindrance at the quinoline moiety causes the rate of the aquation reaction to differ by 3 orders of magnitude between *proximal*- and *distal*-$[Ru(tpy)(pyqu)\ OH_2]^{2+}$.[46]

3.3.2. Photochemical Reactions of proximal-RuEtG. Light irradiation of a *proximal*-**RuEtG** (Figure 8A) solution caused a decrease in the intensity of the doublet peak at 6.69 ppm and the appearance of a singlet peak at 6.65 ppm and a doublet peak at 8.90 ppm (Figure 8C, highlighted with yellow). These new peaks were also observed in the mixture of *proximal*- and *distal*-**RuEtG** (Figure 8B). The minor peak at 6.90 ppm in Figure 8C coincides with the peak of *distal*-**1**. The above spectral changes suggest formation of *distal*-**RuEtG** from *proximal*-**RuEtG**. In this reaction, *distal*-**RuEtG** is supposed to be obtained by (1) the photodissociation of 9-EtG to give *proximal*-**1**, (2) the photoisomerization from *proximal*-**1** to *distal*-**1**, and then (3) the formation of adduct with 9-EtG.

4. CONCLUSIONS

In summary, we have demonstrated substitution reactions of stimuli-responsive metal complexes with the partial structure of a DNA base. The *proximal*-**1** complex formed an adduct in the presence of 9-EtG, as confirmed by ^{1}H NMR, UV−vis, and MS analyses. The *proximal* adduct underwent an isomerization reaction to give the *distal* adduct under visible light irradiation. The metastable complex, *distal*-**1**, showed both thermal back-isomerization to original *proximal*-**1** and adduct formation with 9-EtG at 303 K. Kinetic analysis of the reaction indicated differences in adduct formation between *proximal*-**1** and *distal*-**1**, with 1 order of magnitude. This large difference may arise from steric hindrance and intramolecular hydrogen bonding between a monodentate ligand and a bidentate ligand. The stimuli-responsive nature of the substitution reaction with a model DNA base opens the way to the design of external-stimuli-triggered materials and metallodrugs. The immobilization of the amphiphilic ruthenium complexes to the vesicle, which could lead to the photoresponsive and bioactive vesicles, is currently under study.

■ ASSOCIATED CONTENT

Supporting Information

The Supporting Information is available free of charge at https://pubs.acs.org/doi/10.1021/acsomega.3c05343.

Absorption spectra, ^{1}H and ^{1}H-^{1}H COSY spectra, VT NMR spectra, and ^{1}H NMR spectra of *proximal*-**1**, *proximal*-$[Ru\text{-}(C_2tpy)(C_2pyqu)OH_2]^{2+}$, *proximal*-**RuEtG**, *proximal*-**1** and *distal*-**1**, *proximal*-$[Ru(C_{10}tpy)\text{-}(C_{10}pyqu)Cl]Cl$, and *proximal*-$[\mathbf{1}](NO_3)_2$ (PDF)

■ AUTHOR INFORMATION

Corresponding Author

Masanari Hirahara − *Department of Applied Chemistry, Faculty of Engineering, Osaka Institute of Technology, Osaka 535-8585, Japan*; orcid.org/0000-0001-7765-9995; Phone: 06-6954-4281; Email: masanari.hirahara@oit.ac.jp

Authors

Atsuki Maeda − *Department of Applied Chemistry, Faculty of Engineering, Osaka Institute of Technology, Osaka 535-8585, Japan*

Jun-ya Tokumoto − *Department of Applied Chemistry, Faculty of Engineering, Osaka Institute of Technology, Osaka 535-8585, Japan*

Soichiro Kojima − *Department of Applied Chemistry, Faculty of Engineering, Osaka Institute of Technology, Osaka 535-8585, Japan*

Keiichi Fujimori − *Department of Applied Chemistry, Faculty of Engineering, Osaka Institute of Technology, Osaka 535-8585, Japan*

Takayo Moriuchi-Kawakami − *Department of Applied Chemistry, Faculty of Engineering, Osaka Institute of Technology, Osaka 535-8585, Japan*

Complete contact information is available at: https://pubs.acs.org/10.1021/acsomega.3c05343

https://doi.org/10.1021/acsomega.3c05343
ACS Omega 2023, 8, 37391−37401

Funding

This work was supported by JSPS KAKENHI (grant numbers 20K05456), Yashima Environment Technology Foundation, Kurita Foundation, and JKA promotion (2022M-243).

Notes

The authors declare no competing financial interest.

■ ACKNOWLEDGMENTS

The authors thank Prof. S. Masaoka, Prof. M. Kondo, and Prof. Y. Saga (Osaka University) for kindly supporting the ESI MS spectroscopy measurements. The authors thank Edanz (https://jp.edanz.com/ac) for editing a draft of this manuscript.

■ REFERENCES

(1) Bonnet, S.; Limburg, B.; Meeldijk, J. D.; Klein Gebbink, R. J. M.; Killian, J. A. Ruthenium-Decorated Lipid Vesicles: Light-Induced Release of $[Ru(terpy)(bpy)(OH_2)]^{2+}$ and Thermal Back Coordination. *J. Am. Chem. Soc.* **2011**, *133* (2), 252−261.

(2) Wang, J.; Feringa, B. L. Dynamic Control of Chiral Space in a Catalytic Asymmetric Reaction Using a Molecular Motor. *Science* **2011**, *331* (6023), 1429−1432.

(3) Eisenreich, F.; Kathan, M.; Dallmann, A.; Ihrig, S. P.; Schwaar, T.; Schmidt, B. M.; Hecht, S. A photoswitchable catalyst system for remote-controlled (co) polymerization in situ. *Nat. Catal.* **2018**, *1* (7), 516−522.

(4) Osorio-Planes, L.; Rodríguez-Escrich, C.; Pericàs, M. A. Photoswitchable Thioureas for the External Manipulation of Catalytic Activity. *Org. Lett.* **2014**, *16* (6), 1704−1707.

(5) Blanco-Gómez, A.; Cortón, P.; Barravecchia, L.; Neira, I.; Pazos, E.; Peinador, C.; García, M. D. Controlled binding of organic guests by stimuli-responsive macrocycles. *Chem. Soc. Rev.* **2020**, *49* (12), 3834−3862.

(6) Qu, D.-H.; Wang, Q.-C.; Zhang, Q.-W.; Ma, X.; Tian, H. Photoresponsive Host-Guest Functional Systems. *Chem. Rev.* **2015**, *115* (15), 7543−7588.

(7) Parks, F. C.; Liu, Y.; Debnath, S.; Stutsman, S. R.; Raghavachari, K.; Flood, A. H. Allosteric Control of Photofoldamers for Selecting between Anion Regulation and Double-to-Single Helix Switching. *J. Am. Chem. Soc.* **2018**, *140* (50), 17711−17723.

(8) Einaga, Y.; Sato, O.; Iyoda, T.; Fujishima, A.; Hashimoto, K. Photofunctional Vesicles Containing Prussian Blue and Azobenzene. *J. Am. Chem. Soc.* **1999**, *121* (15), 3745−3750.

(9) Diguet, A.; Yanagisawa, M.; Liu, Y.-J.; Brun, E.; Abadie, S.; Rudiuk, S.; Baigl, D. UV-Induced Bursting of Cell-Sized Multicomponent Lipid Vesicles in a Photosensitive Surfactant Solution. *J. Am. Chem. Soc.* **2012**, *134* (10), 4898−4904.

(10) Li, L.; Rosenthal, M.; Zhang, H.; Hernandez, J. J.; Drechsler, M.; Phan, K. H.; Rütten, S.; Zhu, X.; Ivanov, D. A.; Möller, M. Light-Switchable Vesicles from Liquid-Crystalline Homopolymer-Surfactant Complexes. *Angew. Chem., Int. Ed.* **2012**, *51* (46), 11616−11619.

(11) Jin, Y.; Paris, S. I. M.; Rack, J. J. Bending Materials with Light: Photoreversible Macroscopic Deformations in a Disordered Polymer. *Adv. Mater.* **2011**, *23* (37), 4312−4317.

(12) Li, Q. *Photoactive Functional Soft Materials: Preparation, Properties, and Applications*; Wiley VCH, 2018.

(13) Hirahara, M.; Furutani, S.; Goto, H.; Fujimori, K.; Moriuchi-Kawakami, T. A visible-light and temperature responsive host-guest system: the photoisomerization and inclusion complex formation of a ruthenium complex with cyclodextrins. *Dalton Trans.* **2022**, *51* (11), 4477−4483.

(14) Durham, B.; Wilson, S. R.; Hodgson, D. J.; Meyer, T. J. Cis-Trans Photoisomerization in $[Ru(bpy)_2(OH_2)_2]^{2+}$ - Crystal-Structure of *trans*-$[Ru(bpy)_2(OH_2)(OH)](ClO_4)_2$. *J. Am. Chem. Soc.* **1980**, *102* (2), 600−607.

(15) Yamazaki, H.; Hakamata, T.; Komi, M.; Yagi, M. Stoichiometric Photoisomerization of Mononuclear Ruthenium(II) Monoaquo Complexes Controlling Redox Properties and Water Oxidation Catalysis. *J. Am. Chem. Soc.* **2011**, *133* (23), 8846−8849.

(16) Rack, J. J.; Winkler, J. R.; Gray, H. B. Phototriggered Ru(II)-Dimethylsulfoxide Linkage Isomerization in Crystals and Films. *J. Am. Chem. Soc.* **2001**, *123* (10), 2432−2433.

(17) Juris, A.; Balzani, V.; Barigelletti, F.; Campagna, S.; Belser, P.; Von Zelewsky, A. Ru(II) polypyridine complexes: photophysics, photochemistry, eletrochemistry, and chemiluminescence. *Coord. Chem. Rev.* **1988**, *84*, 85−277.

(18) Nicewicz, D. A.; MacMillan, D. W. C. Merging Photoredox Catalysis with Organocatalysis: The Direct Asymmetric Alkylation of Aldehydes. *Science* **2008**, *322* (5898), 77−80.

(19) Schultz, D. M.; Yoon, T. P. Solar Synthesis: Prospects in Visible Light Photocatalysis. *Science* **2014**, *343* (6174), 1239176.

(20) Alstrum-Acevedo, J. H.; Brennaman, M. K.; Meyer, T. J. Chemical Approaches to Artificial Photosynthesis. 2. *Inorg. Chem.* **2005**, *44* (20), 6802−6827.

(21) Kobayashi, A.; Takizawa, S.-y.; Hirahara, M. Photofunctional molecular assembly for artificial photosynthesis: Beyond a simple dye sensitization strategy. *Coord. Chem. Rev.* **2022**, *467*, 214624.

(22) Ishida, H.; Terada, T.; Tanaka, K.; Tanaka, T. Photochemical carbon dioxide reduction catalyzed by bis(2,2'-bipyridine) dicarbonylruthenium(2+) using triethanolamine and 1-benzyl-1,4-dihydronicotinamide as an electron donor. *Inorg. Chem.* **1990**, *29* (5), 905−911.

(23) Kuriki, R.; Matsunaga, H.; Nakashima, T.; Wada, K.; Yamakata, A.; Ishitani, O.; Maeda, K. Nature-Inspired, Highly Durable CO_2 Reduction System Consisting of a Binuclear Ruthenium(II) Complex and an Organic Semiconductor Using Visible Light. *J. Am. Chem. Soc.* **2016**, *138* (15), 5159−5170.

(24) Richter, M. M. Electrochemiluminescence (ECL). *Chem. Rev.* **2004**, *104* (6), 3003−3036.

(25) Meyer, T. J. Photochemistry of metal coordination complexes: metal to ligand charge transfer excited states. *Pure Appl. Chem.* **1986**, *58* (9), 1193−1206.

(26) White, J. K.; Schmehl, R. H.; Turro, C. An overview of photosubstitution reactions of Ru(II) imine complexes and their application in photobiology and photodynamic therapy. *Inorg. Chim. Acta* **2017**, *454*, 7−20.

(27) Ross, H. B.; Boldaji, M.; Rillema, D. P.; Blanton, C. B.; White, R. P. Photosubstitution in tris chelate complexes of ruthenium(II) containing the ligands 2,2'-bipyrazine, 2,2'-bipyrimidine, 2,2'-bipyridine, and 4,4'-dimethyl-2,2'-bipyridine: energy gap control. *Inorg. Chem.* **1989**, *28* (6), 1013−1021.

(28) Miyazaki, S.; Kojima, T.; Fukuzumi, S. Photochemical and Thermal Isomerization of a Ruthenium(II)-Alloxazine Complex Involving an Unusual Coordination Mode. *J. Am. Chem. Soc.* **2008**, *130* (5), 1556−1557.

(29) Bonnet, S.; Collin, J.-P.; Sauvage, J.-P. Light-Induced Geometrical Changes in Acyclic Ruthenium(II) Complexes and Their Ruthena-Macrocyclic Analogues. *Inorg. Chem.* **2007**, *46* (25), 10520−10533.

(30) Padhi, S. K.; Fukuda, R.; Ehara, M.; Tanaka, K. Photoisomerization and Proton-Coupled Electron Transfer (PCET) Promoted Water Oxidation by Mononuclear Cyclometalated Ruthenium Catalysts. *Inorg. Chem.* **2012**, *51* (9), 5386−5392.

(31) Fomitchev, D. V.; Coppens, P. X-ray Diffraction Analysis of Geometry Changes upon Excitation: The Ground-State and Metastable-State Structures of K2[Ru(NO2)4(OH)(NO)]. *Inorg. Chem.* **1996**, *35* (24), 7021−7026.

(32) Betanzos-Lara, S.; Salassa, L.; Habtemariam, A.; Novakova, O.; Pizarro, A. M.; Clarkson, G. J.; Liskova, B.; Brabec, V.; Sadler, P. J. Photoactivatable Organometallic Pyridyl Ruthenium(II) Arene Complexes. *Organometallics* **2012**, *31* (9), 3466−3479.

(33) Albani, B. A.; Peña, B.; Leed, N. A.; de Paula, N. A. B. G.; Pavani, C.; Baptista, M. S.; Dunbar, K. R.; Turro, C. Marked Improvement in Photoinduced Cell Death by a New Tris-heteroleptic Complex with Dual Action: Singlet Oxygen Sensitization and Ligand Dissociation. *J. Am. Chem. Soc.* **2014**, *136* (49), 17095−17101.

https://doi.org/10.1021/acsomega.3c05343
ACS Omega 2023, 8, 37391−37401

(34) Siewert, B.; van Rixel, V. H. S.; van Rooden, E. J.; Hopkins, S. L.; Moester, M. J. B.; Ariese, F.; Siegler, M. A.; Bonnet, S. Chemical Swarming: Depending on Concentration, an Amphiphilic Ruthenium Polypyridyl Complex Induces Cell Death via Two Different Mechanisms. *Chem.—Eur. J.* **2016**, *22* (31), 10960−10968.
(35) Howerton, B. S.; Heidary, D. K.; Glazer, E. C. Strained Ruthenium Complexes Are Potent Light-Activated Anticancer Agents. *J. Am. Chem. Soc.* **2012**, *134* (20), 8324−8327.
(36) Steinke, S. J.; Gupta, S.; Piechota, E. J.; Moore, C. E.; Kodanko, J. J.; Turro, C. Photocytotoxicity and photoinduced phosphine ligand exchange in a Ru(ii) polypyridyl complex. *Chem. Sci.* **2022**, *13* (7), 1933−1945.
(37) Qu, F.; Park, S.; Martinez, K.; Gray, J. L.; Thowfeik, F. S.; Lundeen, J. A.; Kuhn, A. E.; Charboneau, D. J.; Gerlach, D. L.; Lockart, M. M.; Law, J. A.; Jernigan, K. L.; Chambers, N.; Zeller, M.; Piro, N. A.; Kassel, W. S.; Schmehl, R. H.; Paul, J. J.; Merino, E. J.; Kim, Y.; Papish, E. T. Ruthenium Complexes are pH-Activated Metallo Prodrugs (pHAMPs) with Light-Triggered Selective Toxicity Toward Cancer Cells. *Inorg. Chem.* **2017**, *56* (13), 7519−7532.
(38) Loftus, L. M.; White, J. K.; Albani, B. A.; Kohler, L.; Kodanko, J. J.; Thummel, R. P.; Dunbar, K. R.; Turro, C. New Ru^{II} Complex for Dual Activity: Photoinduced Ligand Release and $^1O_2$ Production$^1O_2$ Production. *Chem.—Eur. J.* **2016**, *22* (11), 3704−3708.
(39) Wachter, E.; Heidary, D. K.; Howerton, B. S.; Parkin, S.; Glazer, E. C. Light-activated ruthenium complexes photobind DNA and are cytotoxic in the photodynamic therapy window. *Chem. Commun.* **2012**, *48* (77), 9649−9651.
(40) Hufziger, K. T.; Thowfeik, F. S.; Charboneau, D. J.; Nieto, I.; Dougherty, W. G.; Kassel, W. S.; Dudley, T. J.; Merino, E. J.; Papish, E. T.; Paul, J. J. Ruthenium dihydroxybipyridine complexes are tumor activated prodrugs due to low pH and blue light induced ligand release. *J. Inorg. Biochem.* **2014**, *130*, 103−111.
(41) Xie, C.; Sun, W.; Lu, H.; Kretzschmann, A.; Liu, J.; Wagner, M.; Butt, H.-J.; Deng, X.; Wu, S. Reconfiguring surface functions using visible-light-controlled metal-ligand coordination. *Nat. Commun.* **2018**, *9* (1), 3842.
(42) Hirahara, M.; Ertem, M. Z.; Komi, M.; Yamazaki, H.; Cramer, C. J.; Yagi, M. Mechanisms of Photoisomerization and Water-Oxidation Catalysis of Mononuclear Ruthenium(II) Monoaquo Complexes. *Inorg. Chem.* **2013**, *52* (11), 6354−6364.
(43) Hirahara, M.; Yagi, M. Photoisomerization of ruthenium(II) aquo complexes: mechanistic insights and application development. *Dalton Trans.* **2017**, *46* (12), 3787−3799.
(44) Hirahara, M.; Goto, H.; Yamamoto, R.; Yagi, M.; Umemura, Y. Photoisomerization and thermal isomerization of ruthenium aqua complexes with chloro-substituted asymmetric bidentate ligands. *RSC Adv.* **2019**, *9* (4), 2002−2010.
(45) Hirahara, M.; Nagai, S.; Takahashi, K.; Saito, K.; Yui, T.; Yagi, M. New Series of Dinuclear Ruthenium(II) Complexes Synthesized Using Photoisomerization for Efficient Water Oxidation Catalysis. *Inorg. Chem.* **2015**, *54* (15), 7627−7635.
(46) Hirahara, M.; Hakamata, T.; League, A. B.; Ertem, M. Z.; Takahashi, K.; Nagai, S.; Inaba, K.; Yamazaki, H.; Saito, K.; Yui, T.; Cramer, C. J.; Yagi, M. Mechanisms and Factors Controlling Photoisomerization Equilibria, Ligand Exchange, and Water Oxidation Catalysis Capabilities of Mononuclear Ruthenium(II) Complexes. *Eur. J. Inorg. Chem.* **2015**, *2015*, 3892−3903.
(47) Hirahara, M.; Goto, H.; Yagi, M.; Umemura, Y. A multi-stimuli responsive ruthenium complex for catalytic water oxidation. *Chem. Commun.* **2020**, *56* (84), 12825−12828.
(48) Hirahara, M.; Tsukamoto, A.; Goto, H.; Tada, S.; Yagi, M.; Umemura, Y. Visible-Light-Induced Morphological Changes of Giant Vesicles by Photoisomerization of a Ruthenium Aqua Complex. *Chem.—Eur. J.* **2016**, *22* (8), 2590−2594.
(49) NOTE: The proximal-/distal- isomers were defined by the structural configuration between a quinoline moiety of pyqu and an aqua ligand.
(50) Poynton, F. E.; Bright, S. A.; Blasco, S.; Williams, D. C.; Kelly, J. M.; Gunnlaugsson, T. The development of ruthenium(ii) polypyridyl complexes and conjugates for in vitro cellular and in vivo applications. *Chem. Soc. Rev.* **2017**, *46* (24), 7706−7756.
(51) Gupta, S.; Vandevord, J. M.; Loftus, L. M.; Toupin, N.; Al-Afyouni, M. H.; Rohrabaugh, T. N., Jr; Turro, C.; Kodanko, J. J. Ru(II)-Based Acetylacetonate Complexes Induce Apoptosis Selectively in Cancer Cells. *Inorg. Chem.* **2021**, *60* (24), 18964−18974.
(52) Corral, E.; Hotze, A. C. G.; Magistrato, A.; Reedijk, J. Interaction between the DNA Model Base 9-Ethylguanine and a Group of Ruthenium Polypyridyl Complexes: Kinetics and Conformational Temperature Dependence. *Inorg. Chem.* **2007**, *46* (16), 6715−6722.
(53) Rilak Simović, A.; Masnikosa, R.; Bratsos, I.; Alessio, E. Chemistry and reactivity of ruthenium(II) complexes: DNA/protein binding mode and anticancer activity are related to the complex structure. *Coord. Chem. Rev.* **2019**, *398*, 113011.
(54) Cuello-Garibo, J.-A.; Meijer, M. S.; Bonnet, S. To cage or to be caged? The cytotoxic species in ruthenium-based photoactivated chemotherapy is not always the metal. *Chem. Commun.* **2017**, *53* (50), 6768−6771.
(55) van Rixel, V. H. S.; Siewert, B.; Hopkins, S. L.; Askes, S. H. C.; Busemann, A.; Siegler, M. A.; Bonnet, S. Green light-induced apoptosis in cancer cells by a tetrapyridyl ruthenium prodrug offering two trans coordination sites. *Chem. Sci.* **2016**, *7* (8), 4922−4929.
(56) Garner, R. N.; Gallucci, J. C.; Dunbar, K. R.; Turro, C. $[Ru(bpy)_2(5\text{-cyanouracil})_2]^{2+}$ as a Potential Light-Activated Dual-Action Therapeutic Agent. *Inorg. Chem.* **2011**, *50* (19), 9213−9215.
(57) Lanquist, A. P.; Gupta, S.; Al-Afyouni, K. F.; Al-Afyouni, M.; Kodanko, J. J.; Turro, C. Trifluoromethyl substitution enhances photoinduced activity against breast cancer cells but reduces ligand exchange in Ru(II) complex. *Chem. Sci.* **2021**, *12*, 12056−12067.
(58) Peña, B.; Saha, S.; Barhoumi, R.; Burghardt, R. C.; Dunbar, K. R. Ruthenium(II)-Polypyridyl Compounds with π-Extended Nitrogen Donor Ligands Induce Apoptosis in Human Lung Adenocarcinoma (A549) Cells by Triggering Caspase-3/7 Pathway. *Inorg. Chem.* **2018**, *57* (20), 12777−12786.
(59) Havrylyuk, D.; Hachey, A. C.; Fenton, A.; Heidary, D. K.; Glazer, E. C. Ru(II) photocages enable precise control over enzyme activity with red light. *Nat. Commun.* **2022**, *13* (1), 3636.
(60) Arora, K.; Herroon, M.; Al-Afyouni, M. H.; Toupin, N. P.; Rohrabaugh, T. N.; Loftus, L. M.; Podgorski, I.; Turro, C.; Kodanko, J. J. Catch and Release Photosensitizers: Combining Dual-Action Ruthenium Complexes with Protease Inactivation for Targeting Invasive Cancers. *J. Am. Chem. Soc.* **2018**, *140* (43), 14367−14380.
(61) van Vliet, P. M.; Haasnoot, J. G.; Reedijk, J. Binding of 9-Methylhypoxanthine and 9-Ethylguanine to $[cis\text{-}Ru(2,2'\text{-bipyridine})_2]^{2+}$. NMR and X-ray Structure of *cis*-Chlorobis(2,2'-bipyridine)-(9-ethylguanine-κ-N7) ruthenium(II) Chloride. *Inorg. Chem.* **1994**, *33* (9), 1934−1939.
(62) Zobi, F.; Hohl, M.; Zimmermann, I.; Alberto, R. Binding of 9-Methylguanine to $cis\text{-}[Ru(2,2'\text{-bpy})_2]^{2+}$: First X-ray Structure of a *cis*-Bis Purine Complex of Ruthenium. *Inorg. Chem.* **2004**, *43* (9), 2771−2772.
(63) Melchart, M.; Habtemariam, A.; Parsons, S.; Sadler, P. J. Chlorido-aqua-9-ethylguanine- and 9-ethyladenine-adducts of cytotoxic ruthenium arene complexes containing O,O-chelating ligands. *J. Inorg. Biochem.* **2007**, *101* (11−12), 1903−1912.
(64) NOTE: The apparent molecular weight (3640 g/mol) was calculated based on a 1:21 ratio of C_{10}pyqu (M.W. = 362.5) and 1-decanol (MW = 158.3).
(65) Menges, F. *Spectragryph—optical spectroscopy software*; 1.2; Germany, 2017.
(66) Huynh, M. H. V.; Lasker, J. M.; Wetzler, M.; Mort, B.; Szczepura, L. F.; Witham, L. M.; Cintron, J. M.; Marschilok, A. C.; Ackerman, L. J.; Castellano, R. K.; Jameson, D. L.; Churchill, M. R.; Jircitano, A. J.; Takeuchi, K. J. Remarkable Spectator Ligand Effect on the Rate Constant of Ligand Substitution of (Aqua) ruthenium(II) Complexes. *J. Am. Chem. Soc.* **2001**, *123* (36), 8780−8784.

https://doi.org/10.1021/acsomega.3c05343
ACS Omega 2023, 8, 37391−37401

(67) Bessel, C. A.; Margarucci, J. A.; Acquaye, J. H.; Rubino, R. S.; Crandall, J.; Jircitano, A. J.; Takeuchi, K. J. Steric ligand effects of six bidentate bipyridyl ligands. *Inorg. Chem.* **1993**, *32* (25), 5779−5784.

https://doi.org/10.1021/acsomega.3c05343
ACS Omega 2023, 8, 37391−37401